Title: Thermal synthesis of Hematite nanoparticles : structural, magnetic and morphological characterizations

Author: Anubha Dey, Maciej Zubko, Joachim Kusz, Varimalla Raghavendra Reddy, Alok Banerjee, Ashis Bhattacharjee

Int. J. Nano Dimens., 11 (2): 188-198, Spring 2020

ORIGINAL ARTICLE

Thermal synthesis of Hematite nanoparticles: Structural, magnetic and morphological characterizations

Anubha Dey[1], Maciej Zubko[2,3], Joachim Kusz[4], Varimalla Raghavendra Reddy[5], Alok Banerjee[5], Ashis Bhattacharjee[1,]*

[1]*Department of Physics, Institute of Science, Visva-Bharati University, Santiniketan, 731235, India.*
[2]*Institute of Material Science, University of Silesia, Poland.*
[3]*Department of Physics, University of Hradec Králové, Czech Republic.*
[4]*Institute of Physics, University of Silesia, Katowice,Poland.*
[5]*UGC-DAE Consortium for Scientific Research, Mossbauer and MOKE laboratory, Indore, India.*

Received 18 December 2019; revised 01 April 2020; accepted 08 April 2020; available online 17 April 2020

Abstract

Hematite (α-Fe_2O_3) nanoparticle was synthesized using organometallic compound - ferrocene carboxaldehyde through solventless solid state thermal decomposition technique. The crystal structure, magnetic and morphological properties of the decomposed material were studied using powder X-ray diffraction (XRD), superconducting quantum interference device (SQUID) magnetometry, ^{57}Fe Mössbauer spectroscopy, scanning electron microscopy (SEM), transmission electron microscopy (TEM) and energy-dispersive X-ray spectroscopy (EDX) techniques. Structural study confirmed that the synthesized material is hematite with hexagonal phase and good crystallinity. The temperature-dependent magnetization measurement exhibited the Morin transition - the yardstick for hematite formation. Mössbauer spectroscopic study confirmed the purity of phase of the synthesized material. The SEM study observed mostly the agglomerated tiny particles along with some ring-shaped surface structures. The TEM study of the synthesized material showed that the highest distribution of the particles with ~5 nm size. The observed EDX spectra confirmed the existence of Fe and O in the synthesized material. The solid state reaction process leading to hematite on decomposition of ferrocene carboxaldehyde has also been proposed. Present study describes a simple process for the preparation of pure hematite nanoparticle by solventless method.

Keywords: *Characterization; Ferrocene Carboxaldehyde; Hematite; Nanoparticle; Thermal Synthesis.*

How to cite this article

Dey A, Zubko M, Kusz J, Raghavendra Reddy V, Banerjee A, Bhattacharjee A. Thermal synthesis of Hematite nanoparticles: Structural, magnetic and morphological characterizations. Int. J. Nano Dimens., 2020; 11 (2): 188-198.

INTRODUCTION

Hematite (α-Fe_2O_3) - a nontoxic and environmentally compatible n-type semiconductor is the most stable iron oxide under ambient conditions. This material has attracted considerable research attention for many years owing to its physical properties and wide application potential in the fields like, magnetic devices, catalysis, pigments, gas sensors, photo anodes, batteries [1–7]. Magnetism observed in hematite is interesting and is widely discussed in the scientific literature [8]. Below ~260 K (Morin transition temperature), hematite becomes anti-ferromagnetic as spins are arranged in anti-parallel fashion along the rhombohedral (111) axis, whereas above 260 K a canted spin arrangement with respect to the basal (111) plane gives rise to a weak ferromagnetism in hematite [9, 10]. Since last several years, efforts are given to synthesize hematite nanomaterials of different size and morphology to enhance/improve their performance in various applications. Various types of hematite nanoparticles with different morphology have been developed: nanocrystals [11], polyhedral nanoparticle [12], nanorods [13],

* Corresponding Author Email:
ashis.bhattacharjee@visva-bharati.ac.in

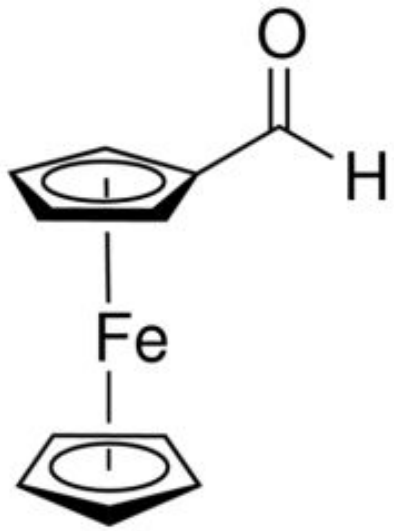

Fig. 1. Schematic diagram of ferrocene carboxaldehyde, ($C_{11}H_{10}FeO$).

nanoribbons [14], nanotubes [15], nanostructured microspheres [16], hollow nanostructures [17] and nanoplates [18]. Various methods, including thermal decomposition [19], sol–gel [20], ionic liquid-assisted synthesis [21], hydrothermal method [22], co-precipitation method [23] and solvent-less growth [24] have been developed to synthesize hematite nanoparticle. Among these methods, the technique of thermal decomposition becomes increasingly important as recent developments in the preparation of iron oxide nanoparticle by thermal decomposition of iron containing complexes have significantly improved the quality of traditional iron oxide nanoparticle in terms of size tunability, monodispersity and crystalline structure [19, 25–29]. However, the ease of synthesis through thermal decomposition is limited owing to the toxicity, complexity of the decomposition reaction and air-sensitivity of the precursors as well as the requirement of high reaction temperatures. These led the synthesis of stable iron oxide nanoparticles with controlled size from suitable precursors through simple reaction procedures to remain challenging [30].

Among the iron-based organic precursors used for thermal decomposition reported so far, ferrocene or bis(η^5-cyclopentadienyl)iron, [Fe(η^5-C_5H_5)$_2$] remained interesting precursor for the control growth of the nanoparticles [19, 27, 31–42]. To the best of our knowledge, there are only two reports on the experimental study of thermal decomposition of ferrocene [19,34]. Earlier, it has been reported that ferrocene on heating undergoes sublimation at ~483K, but when heated in presence of oxalic acid, yields hematite nanoparticle (~40 nm) due to thermal decomposition at ~453K [19]. Continuing the search for suitable iron-based organic precursors, we have extended our investigations with ferrocene derivatives, and reported the formation of hematite nanoparticles on thermal decomposition of acetyl ferrocene [43] and the kinetics of thermal decomposition reaction [44]. In this light, presently we report the solventless synthesis of hematite nanoparticle by thermally decomposing another ferrocene derivative - ferrocene carboxaldehyde. The structural, magnetic and morphological characterizations of the decomposed material along with a proposed reaction pathway are presented in the present paper. The solventless thermal decomposition method provides a new concept for the synthesis of other metal oxide nanomaterials owing to the simplicity of the process.

MATERIALS AND METHODS

Materials

Ferrocene carboxaldehyde ($C_{11}H_{10}FeO$) (Fig. 1) was purchased from Sigma-Aldrich and this organoiron compound was used for solventless solid state thermal decomposition as a precursor. The thermal decomposition was carried out inside a thermogravimetric analyzer (STA 449 F3 Jupiter of Netzsch, Germany) with UHP

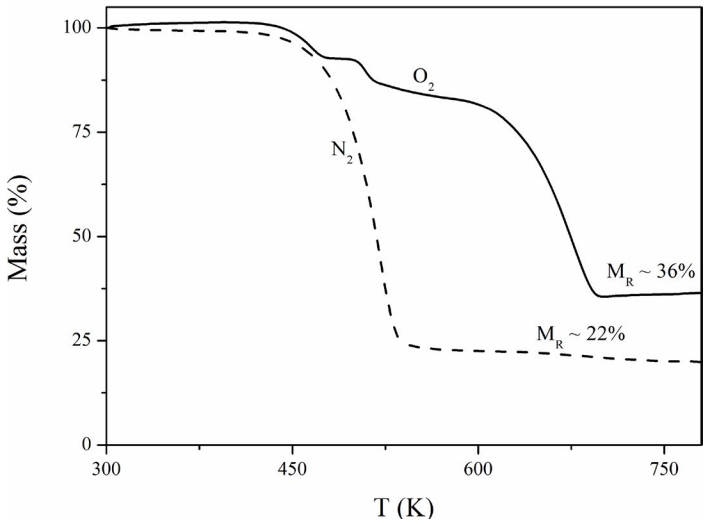

Fig. 2. Thermogravimetry profile of ferrocene carboxaldehyde in oxygen atmosphere.

(99.999%) nitrogen (N_2) and oxygen (O_2) gases as the reaction environments. In each case of reaction environments, the thermogravimetry was continued till the thermal decomposition of the precursor was complete. UHP (99.999%) nitrogen gas was used as the protective gas in the instrument. The crucible used for the decomposition study was made of alumina. The residual materials obtained after the completion of decomposition of the precursor in nitrogen and oxygen gas atmospheres, hereafter denoted as Fc-N and Fc-O accordingly, were collected for physical characterizations.

Methods

The decomposed materials were studied with various physical characterization techniques like powder X-ray diffraction (XRD), superconducting quantum interference device (SQUID) magnetometry, ^{57}Fe Mössbauer spectroscopy, scanning electron microscopy (SEM), transmission electron microscopy (TEM) and energy-dispersive X-ray spectroscopy (EDX). The XRD study was done with PANalytical's Emperian powder diffractometer equipped with PIXcell^{3D} detector with a Cu-K_α radiation source. The XRD data were analyzed by the Rietveld method using the FullProf program. The average crystallite size (D) of the samples was estimated from the XRD patterns using the Scherer formula [45]:

$$D = \frac{K\lambda}{\beta \cos\theta}$$

where D is the crystallite size of the hematite nanoparticle (in nm), K is a constant related to the crystallite shape (K = 0.9), λ is the wavelength of Cu-K_α radiation, β is the full width at half maximum (FWHM) of the diffraction peak (in radians) and ϑ is the diffraction angle (in radians). The mean crystallite size was estimated based on the full pattern analysis. The magnetic property was investigated by a SQUID magnetometer (MPMS, Quantum Design) under the applied magnetic field of 0.1 Tesla sweeping in 300 K – 10 K – 300 K temperature cycle. ^{57}Fe Mössbauer spectra were recorded using a conventional constant-acceleration spectrometer with a ^{57}Co Mössbauer source. The morphologies and particle sizes of the synthesized material were studied by scanning electron microscopy (SEM) and transmission electron microscopy (TEM). The EDX study was made to identify the elements present in the material produced. The SEM observations were performed using JEOL JSM-6480 instrument with accelerating voltage of 20 kV equipped with the EDX detector from IXRF. The TEM observations were performed using a JEOL JEM 3010 instrument with 300 kV accelerating voltage equipped with 2k×2k OriusTM 833 SC200D Gatan CCD camera.

RESULTS AND DISCUSSIONS

Thermogravimetry

Iron oxides were produced by thermal decomposition of ferrocene carboxaldehyde in nitrogen and oxygen reaction atmospheres inside a thermogravimetric analyzer. Fig. 2

shows the thermal behaviour of the precursor under two different reaction atmospheres. The thermogravimetry profile of the precursor in nitrogen atmosphere shows that the thermal decomposition, initiated at ~420K followed by a single step process with maximum thermal decomposition occurring at ~520K, was completed at ~560K leaving 22% residual mass (Fc-N). On the other hand, the thermal decomposition in oxygen atmosphere, initiated at the same temperature but followed by a three-step process, was completed at ~700K leaving 36% residual mass (Fc-O). The significant differences noted in these two thermogravimetry profiles of ferrocene carboxaldehyde obtained in inert and oxidative atmospheres reflect the role of the reaction atmosphere on the solid state reaction of the precursor.

It is to be noted here that in inert atmosphere the sublimation of ferrocene initiates at ~400 K and thermal decomposition of ferrocene in the presence of oxalic acid starts at ~335 K [19], while thermal decomposition of ferrocene carboxaldehyde initiates at ~420 K. Acetyl ferrocene with substituted $–COCH_3$ group decomposes at ~450K [43]. On analysis of the presently observed thermogravimetry results, substitution of aldehyde (–CH=O) group on one of the cyclopentadienyl rings of ferrocene molecule restricts the sublimation process and increases the overall thermal stability of the compound by elevating the thermal decomposition temperature both in nitrogen and oxygen atmospheres in comparison to that of ferrocene.

Structural analysis

The phase and structure of the decomposed materials - Fc-N and Fc-O were identified using powder X-ray diffraction technique at room temperature. Fig. 3 represents the room temperature powder XRD patterns of Fc-N and Fc-O. The observed XRD patterns have been found to match with the standard JCPDS nos. 24-72 and 13-534, 89-2867 and 00-065-0731 for hematite, cementite and magnetite, respectively for Fc-N and with the standard JCPDS nos. 24-72 and 13-534 for Fc-O. The Rietveld refinements of the XRD profiles are shown in Fig. 3 where the dots represent the observed data and the lines correspond to the calculated patterns. The curves at the bottom represent the difference between the observed and calculated patterns. The vertical bars show the Bragg diffraction positions. From the analysis of the XRD pattern for Fc-N, we find that it is a multiphase material where the phases are hematite (15.8%), cementite (43.3%) and magnetite (40.8%). Apart from these, a broad and intense peak at $2\theta = 26^{o}$ was observed which may be assigned to the formation of graphite. The formation of the graphite phase of carbon during thermal decomposition has often been reported owing to the catalysis of the elementary iron nanoparticles [46,47]. The average crystallite size *D* calculated using Scherer formula for hematite, cementite and magnetite are 85.0 nm, 41.2 nm and 13.5 nm, respectively.

On the other hand, for Fc-O a close agreement between the observed and calculated XRD patterns establishes the single-phase formation of the material in the hexagonal structure of hematite with $R\bar{3}$-3c space group. The refined cell parameters for Fc-O are as follows: a = 5.0349(1) Å, c = 13.7450(3) Å which are in good agreement with the reference patterns JCPDF nos. 24-72 and 13-534. The diffraction peaks corresponding to (012), (104), (110), (113), (024), (116), (018), (214), (300), and (220) planes are in good relationship with the standard XRD pattern of hematite structure. No other peak owing to other crystal phase or impurity was observed in the recorded XRD pattern, which reveals that the synthesized Fc-O material consists of pure α-Fe_2O_3 phase. The average crystallite size *D* calculated using Scherer formula is 561.8(3) nm.

As we are interested in the iron oxides available in pure phase only, in the following sections we will discuss the characterization studies carried out for Fc-O only.

Magnetic studies

Fig. 4 represents the temperature dependence of magnetization (M) for Fc-O in the 300 K-10 K-300 K temperature cycle obtained from SQUID measurements. From this figure, one can see that while cooling, the M value starts with slight increase (0.043 emu/gm to 0.045emu/gm) followed by a rapid decrease at ~260 K which continues until ~240 K and then M value very slowly decreases (~0.033 emu/gm) with decreasing temperature. On the other hand, while heating the $M(T)$ plot retraces the same path till ~240 K and then increases rapidly above ~240 K till 270 K. On heating above this temperature up to room temperature (300 K), the $M(T)$ value

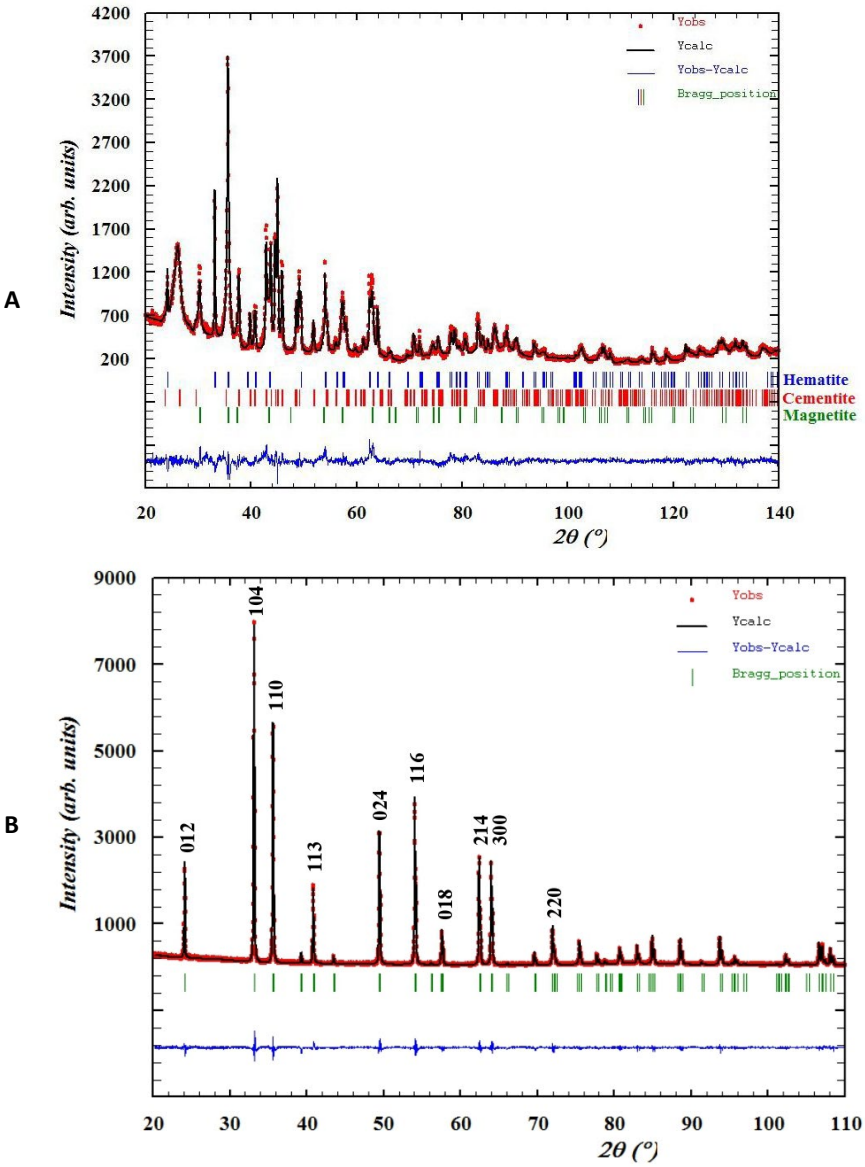

Fig. 3. Powder XRD pattern of the residue materials obtained on thermal decomposition of ferrocene carboxaldehyde in different atmospheres: (a) nitrogen, (b) oxygen.

gradually increases tending towards a near saturation value (0.062 emu/gm). Thus, the present *M*(*T*) plots indicate a magnetic transition around ~260 K during cooling-heating cycle which can be easily recognized as Morin transition [9] - the characteristic behaviour of hematite. Thus, Fc-O is hematite which is in complete agreement with the result observed from XRD study.

With thermal cycling, i.e., cooling →heating, there has been a constant (~14%) increase in magnetization values at 300 K for Fc-O. The irreversible changes observed in the M(T) plots as well as in the magnetization values with thermal cycling may be due to domain reorganization [48,49]. Thermal cycling through Morin temperature modifies the domain configuration. Most of the hematite crystals lose their domain pattern on cooling [50]. A single-domain state is often observed below the Morin temperature, and if this is warmed to room temperature again, a new domain pattern is seen. Consecutive thermal cycling ultimately gives rise to a stable domain at

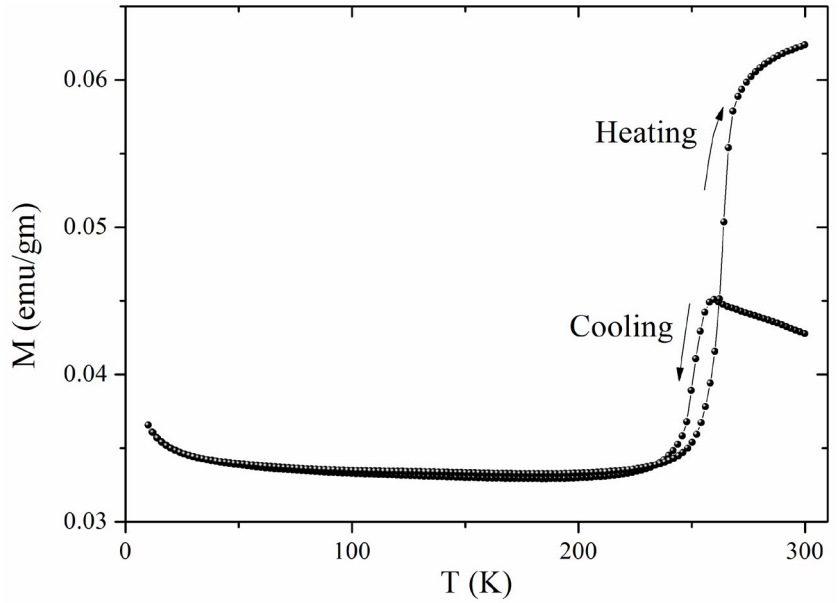

Fig. 4. Temperature dependence of magnetization (M) of the decomposed material (Fc-O) under 0.1 Tesla magnetic fields in a cooling and heating cycle.

room temperature for hematite [49].

When compared with the saturation magnetization values of hematite available in the literature (ranges from 0.03 emu/gm [51] to 5.1 emu/gm [52]), the room temperature magnetization (tending towards saturation) value (0.06 emu/gm) observed for Fc-O after heating is low. This low value of magnetization observed may be due to fact that different synthetic methods provide different particle sizes, morphologies and surface structures which significantly affect the magnetic properties of the materials obtained.

^{57}Fe Mössbauer spectroscopy enables one to identify the iron compound(s) present in a sample as constituent(s) as well as provides a quantitative estimation of the iron site(s) in the solid [53]. Each such magnetic constituent, depending upon their spin state, gives different component in the Mössbauer spectrum. Analysis of such spectra leads to the identification of different iron containing constituent compounds present in the sample. In this light, ^{57}Fe Mössbauer spectra of Fc-O was recorded at room temperature (Fig. 5) to confirm the existence of only hematite – the magnetic constituent in Fc-O as seen through XRD and magnetic studies. The Mössbauer spectrum was fitted to Lorenzian line with isomer shift with respect to α-iron (δ), quadrupole interaction (ΔE_Q), hyperfine field (B_{hf}) and the line width as the adjustable parameters for the spectral fits. The observed spectrum for Fe-O is well fitted with a single sextet. The sextet indicates the presence of long-range magnetic order in this sample at the measured temperature. The estimated hyperfine parameters are: isomer shift = 0.37 ± 0.01 mm/s, quadrupole splitting = -0.19 ± 0.01 mm/s and hyperfine field = 51.7 ± 0.03 Tesla. These hyperfine parameter values correspond to Fe^{3+} in a hematite structure [19,54]. The appearance of single sextet confirms the presence of pure phase of hematite in Fc-O. Thus, the Mössbauer spectroscopic study confirms that the thermally synthesized material Fc-O is purely hematite in complete agreement with the XRD and SQUID results.

SEM, EDX and TEM observations

The surface morphology of Fc-O sample was studied using SEM. The SEM images obtained at different regions of the sample surface under different magnifications are shown in Figs 6. It is seen that the most of the surface is covered with thin ring shaped structures (Fig. 6a) whereas in rest of the surface there are agglomeration of many tiny particles mostly having round edges (insert of Fig. 6a). The ring-shaped objects, when sampled over twenty species, are found to have average

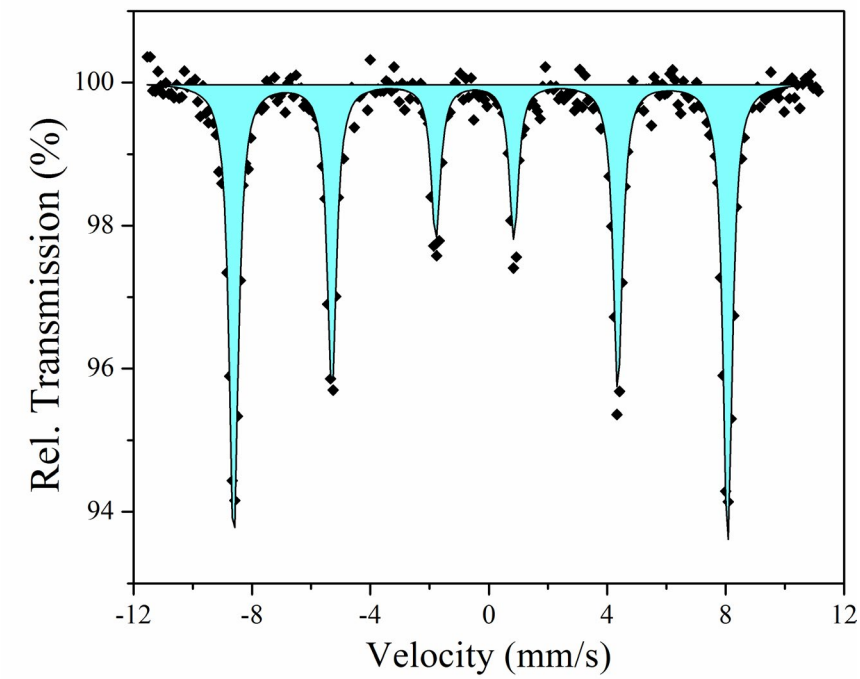

Fig. 5. ^{57}Fe Mössbauer spectrum of the decomposed material (Fc-O) recorded at room temperature.

inner and outer diameter as 0.08µm and 2.08µm, respectively. In some areas of the sample surface, the tiny particles are arranged in chain-like fashion (Fig. 6b). The size distribution and the morphologies of Fc-O sample were irregular in nature and found to represent relatively rough surfaces with a dense and non-uniformly distributed various sized grains (Fig. 6c). The different morphologies observed from SEM images may be due to differences in the local reaction environment and/or cooling process.

In order to identify the elements present in the different surface areas of the sample, the EDX spectrum was obtained from different parts of the SEM images. Circular spots on the SEM images of Fig. 6 are some of the selected areas from where EDX spectrum was taken. A representative EDX spectrum is shown as Fig. 6d. It has been noted that all such spectra exhibited characteristic peaks for Fe and O only at the same positions although there are slight differences in the intensity. Thus, the EDX study confirms that the obtained nanoparticles are pure in nature.

The particle size of the Fc-O sample was determined by TEM analysis. The TEM images of Fc-O were obtained at different resolutions. Figs. 7a and 7b represent two selected TEM images at different resolutions from where it is clear that Fc-O material consists of agglomeration of tiny dots of various shapes and sizes and the diameter of the smallest particles lie in the nanometre range. From the particle size histogram created from the TEM image analysis shown as insert of Fig. 7, the average particle size is found to be ~5nm. The large difference in the particle size obtained from TEM study and the average crystallite size using XRD data analysis should be due to agglomeration as is evidenced. Analysis of the average crystallite size from the XRD data uses the broadening of the diffraction lines in the well-known Scherer formula. This formula is rather poor when it comes to the particles of sizes above 50 nm. One can always get a result as it is a mathematical formula, but the result should be meaningful. There can be challenges when it comes to agglomerates and aggregates. TEM allows to measure every particle individually, therefore is less statistical.

Possible solid state reaction

Ferrocene has a “sandwich structure” of two parallel cyclopentadienyl rings with an iron in the centre between these rings while ferrocene carboxaldehyde is a substituted ferrocene derivative. It is known that ferrocene sublimates at

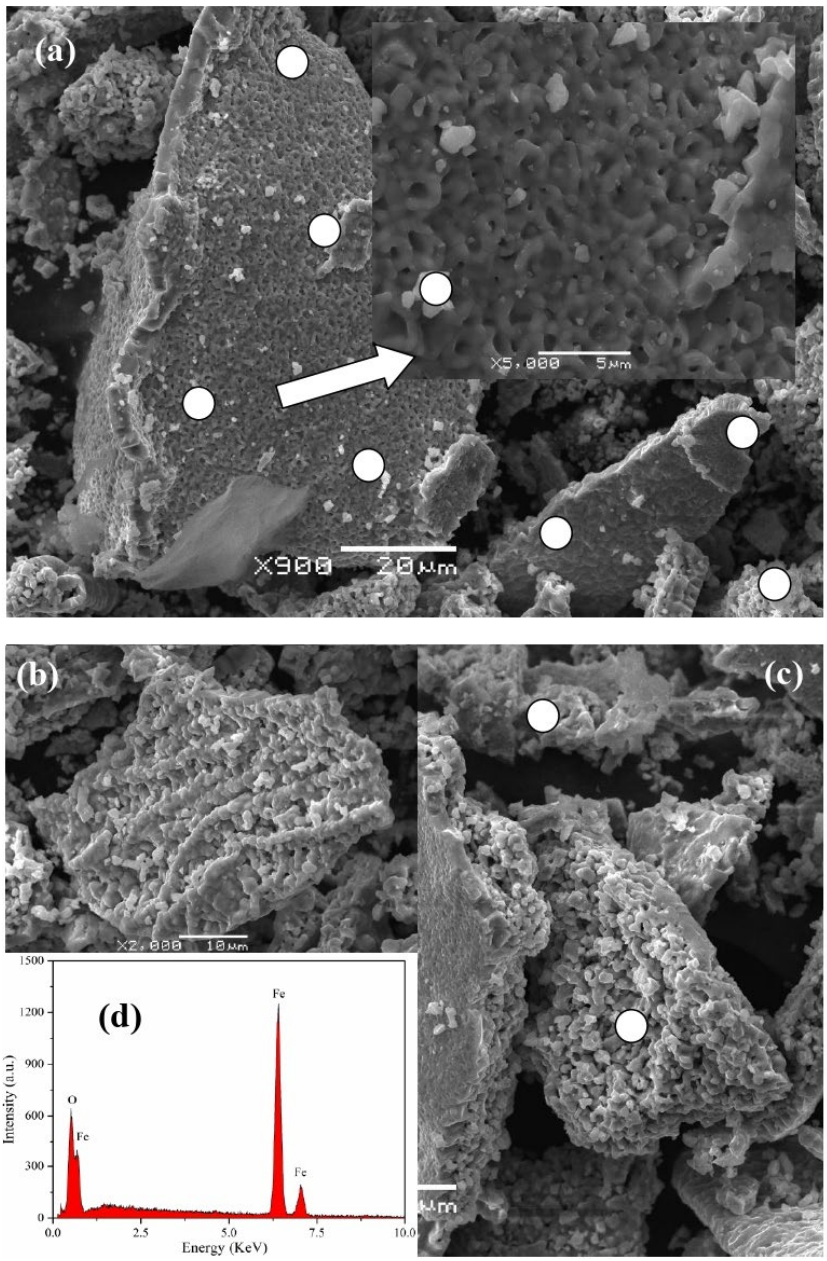

Fig. 6. SEM images of the decomposed material (Fc-O): (a) the sample surface is covered with thin ring shaped structures; (b) the tiny particles arranged in chain-like fashion; (c) non-uniformly distributed various sized grains; (d) EDX spectrum. The white spots on the SEM images indicate the areas where the EDX studies were made.

448 K and at temperatures above ~773 K, gaseous ferrocene decomposes spontaneously to form metallic iron and some volatile gases e.g., H_2, CH_4, C_5H_6. [41]. Considering the strength of the different bonds present in ferrocene carboxaldehyde, it is quite obvious that before the breakage of the Fe-C bonds, the –CH=O bond will break. Thus, at this temperature range solid or liquid-like iron particles are present in the reaction medium and the metallic iron will then react with the available oxygen giving rise to hematite [41]. Angermann and Töffer [55] reported the formation of hematite through thermal decomposition of iron oxalate in air atmosphere. From the characterization studies of the decomposed material Fc-O obtained from ferrocene carboxaldehyde, it is understood that

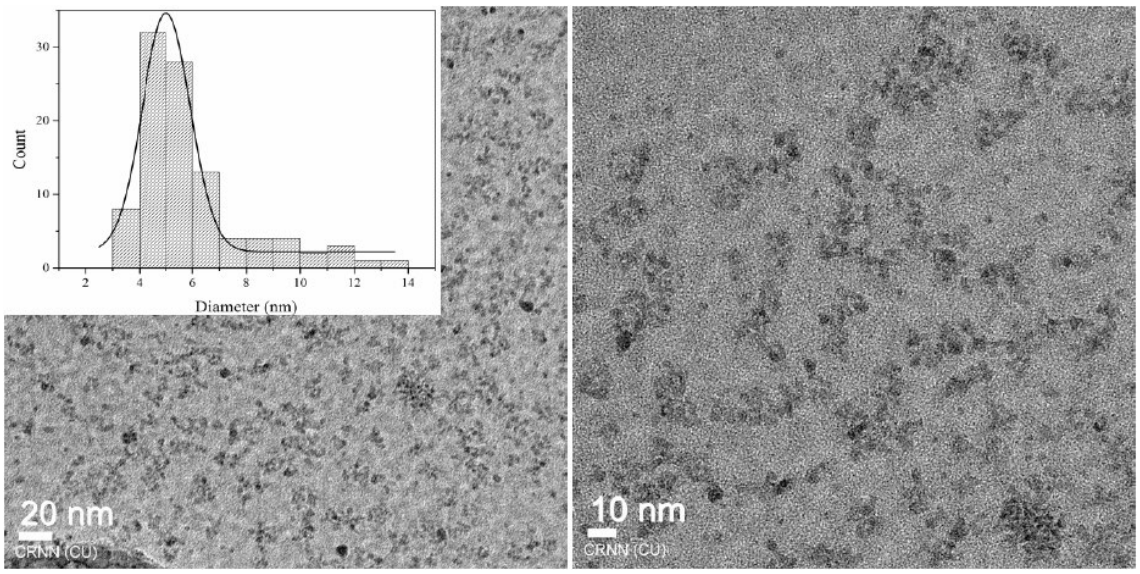

Fig. 7. TEM images of the decomposed material (Fc-O) at two different resolutions. Insert shows the particle size histogram.

on heating ferrocene carboxaldehyde in oxygen atmosphere at ~800 K completely decomposes to hematite. Considering the compositional analysis of the decomposed material obtained from the XRD and EDX studies and the amount of iron concentration in the material as seen through Mössbauer spectroscopy, the possible thermal decomposition reaction of ferrocene carboxaldehyde in oxygen may be understood through the following equation:

$4C_{11}H_{10}FeO + 45O_2\,(g) \rightarrow 2Fe_2O_3 + 44CO_2\,(g) + 20H_2\,(g)$

where 'g' and 's' denote gaseous and solid substances, respectively. The observed residual mass from the thermogravimetry profile is 36.85%, whereas the calculated value of residual mass from the proposed reaction pathway is 37.3%. Thus, the proposed reaction pathway indicates the formation of α-Fe_2O_3 (hematite) as a result of decomposition of ferrocene carboxaldehyde completed at ~800 K. CO, if produced during the reaction, may be deoxidized to oxygen and carbon by metallic iron liberated from thermal decomposition of ferrocene carboxaldehyde [56] and the metallic iron in turn then reacts with the liberated oxygen giving rise to hematite. This may be an additional reaction leading to hematite. The observed Mössbauer spectrum of Fc-O did not exhibit any trace of iron carbide (Fe_3C) or free iron (Fe). Thus, the proposed reaction correctly leads to the formation of hematite (α-Fe_2O_3) due to thermal decomposition of ferrocene carboxaldehyde in oxygen atmosphere.

CONCLUSIONS

Hematite (α-Fe_2O_3) nanoparticle with average size of ~5 nm has been successfully synthesized by solid state thermal decomposition of ferrocene carboxaldehyde in oxidative atmosphere. The structural, magnetic and morphological properties of the synthesized sample were studied. The observed XRD pattern confirmed that the material corresponds to the pure hematite phase. The temperature dependent magnetic measurements of the material exhibited the Morin transition confirming the hematite nature of the synthesized sample. Room temperature Mössbauer spectroscopic study supplemented the existence of single phase hematite in the material produced. The present study describes a novel and simple process for the preparation of pure hematite nanoparticle. On the other hand, the study also enlightens the effect of reaction atmosphere on the thermal synthesis. In order to unearth the nature of the undergoing solid state reaction in the thermal decomposition of ferrocene carboxaldehyde under oxygen and nitrogen atmospheres, study on the kinetics of reaction is getting our interest. Considering the presently observed results, the solventless

thermal decomposition of metal-containing organic complexes may be a suitable method for preparing metal oxide nanomaterials.

ACKNOWLEDGEMENTS

Author AD is thankful to DST-INSPIRE, Govt of India for providing a fellowship. AD acknowledges UGC-DAE CSR, Indore, India, for providing financial assistance to carry out magnetic and Mössbauer measurements. Financial support for the thermogravimetry analyzer (STA 449 F3 Jupiter) from the Department of Science and Technology (DST), Govt. of India through a grant (Ref. No. SR/FIST/PSI-157/2010) to the Department of Physics, Visva-Bharati University is gratefully acknowledged.

CONFLICT OF INTEREST

The authors declare that they have no competing interests.

REFERENCES

1. Mor G. K., Prakasam H. E., Varghese O. K., Shankar K., Grimes C. A., (2007), Vertically oriented Ti− Fe− O nanotube array films: Toward a useful material architecture for solar spectrum water photoelectrolysis. *Nano Lett.* 7: 2356–2364.
2. El-Sheikh S. M., Harraz F. A., Abdel-Halim K. S., (2009), Catalytic performance of nanostructured iron oxides synthesized by thermal decomposition technique. *J. Alloys Compd.* 487: 716–723.
3. Salazar-Alvarez G., Qin J., Sepelak V., Bergmann I., Vasilakaki M., Trohidou K. N., Ardisson J. D., Macedo W. A. A., Mikhaylova M., Muhammed M., (2008), Cubic versus spherical magnetic nanoparticles: The role of surface anisotropy. *J. Am. Chem. Soc.* 130: 13234–13239.
4. Tseng W. J., Lin R. -D., (2014), $BiFeO_3$/ α-Fe_2O_3 core/shell composite particles for fast and selective removal of methyl orange dye in water. *J. Colloid Interf. Sci.* 428: 95–100.
5. Cesar I., Kay A., Gonzalez Martinez J. A., Grätzel M., (2006), Translucent thin film Fe_2O_3 photoanodes for efficient water splitting by sunlight: Nanostructure-directing effect of Si-doping. *J. Am. Chem. Soc.* 128: 4582–4583.
6. Jain G., Balasubramanian M., Xu J. J., (2006), Structural studies of lithium intercalation in a nanocrystalline α-Fe_2O_3 compound. *Chem. Mater.* 18: 423–434.
7. Colombo C., Palumbo G., DiIorio E., Song X., Jiang Z., Liu Q., Angelico R., (2015), Influence of hydrothermal synthesis conditions on size, morphology and colloidal properties of Hematite nanoparticles. *Nano-Structures & Nano-Objects*. 2: 19–27.
8. Tadić M., Marković D., Spasojević V., Kusigerski V., Remškar M., Pirnat J., Jagličić Z, (2007), Synthesis and magnetic properties of concentrated α-Fe_2O_3 nanoparticles in a silica matrix. *J. Alloys Compd.* 441: 291–296.
9. Morin F. J., (1950), Magnetic susceptibility of α-Fe_2O_3 and α-Fe_2O_3 with added titanium. *Phys. Rev.* 78: 819-826.
10. Adler D., (1968), Insulating and metallic states in transition metal oxides. *Solid state Phys.* (Elsevier), 21: 1–113.
11. Manukyan K. V., Chen Y.-S., Rouvimov S., Li P., Li X., Dong S., Liu X., Furdyna J. K., Orlov A., Bernstein G. H., (2014), Ultrasmall α-Fe_2O_3 superparamagnetic nanoparticles with high magnetization prepared by template-assisted combustion process. *J. Phys. Chem. C*. 118: 16264–16271.
12. Lin M., Tng L., Lim T., Choo M., Zhang J., Tan H.R., Bai S., (2014), Hydrothermal synthesis of octadecahedral hematite (α-Fe_2O_3) nanoparticles: An epitaxial growth from goethite (α-FeOOH). *J. Phys. Chem. C*. 118: 10903–10910.
13. Lin Y.-M., Abel P. R., Heller A., Mullins C. B., (2011), α-Fe_2O_3 nanorods as anode material for lithium ion batteries. *J. Phys. Chem. Lett.* 2: 2885–2891.
14. Sarkar D., Mandal M., Mandal K., (2013), Design and synthesis of high performance multifunctional ultrathin hematite nanoribbons. *ACS Appl. Mater. Interf*. 5: 11995–12004.
15. Jia C., Sun L., Yan Z., You L., Luo F., Han X., Pang Y., Zhang Z., Yan C., (2005), Single crystalline iron oxide nanotubes. *Angew. Chemie Int. Ed.* 44: 4328–4333.
16. Liu X., Wang H., Su C., Zhang P., Bai J., (2010), Controlled fabrication and characterization of microspherical $FeCO_3$ and α-Fe_2O_3. *J. Colloid Interf. Sci.* 351: 427–432.
17. Kwon K.-A., Lim H.-S., Sun Y.-K., Suh K.-D., (2014), α-Fe_2O_3 submicron spheres with hollow and macroporous structures as high-performance anode materials for lithium ion batteries. *J. Phys. Chem. C*. 118: 2897–2907.
18. Cai J., Chen S., Ji M., Hu J., Ma Y., Qi L., (2014), Organic additive-free synthesis of mesocrystalline hematite nanoplates via two-dimensional oriented attachment. *Cryst. Eng. Comm*. 16: 1553–1559.
19. Bhattacharjee A., Rooj A., Roy M., Kusz J., Gütlich P., (2013), Solventless synthesis of hematite nanoparticles using ferrocene. *J. Mater. Sci.* 48: 2961–2968.
20. Kayani Z. N., Afzal A., Butt M. Z., Batool I., Arshad S., Ali Y., Riaz S., Naseem S., (2015), Structural, optical and magnetic properties of iron oxide nano-particles. *Mater. Today Proc.* 2: 5660–5663.
21. Xu L., Xia J., Wang K., Wang L., Li H., Xu H., Huang L., He M., (2013), Ionic liquid assisted synthesis and photocatalytic properties of α-Fe_2O_3 hollow microspheres. *Dalt. Trans.* 42: 6468–6477.
22. Khalil N. M., Wahsh M. M. S., Saad E. E., (2015), Hydrothermal extraction of α-Fe_2O_3 nanocrystallite from hematite ore. *J. Ind. Eng. Chem.* 21: 1214–1218.
23. Farahmandjou M., Soflaee F., (2015), Synthesis and characterization of α-Fe_2O_3 nanoparticles by simple co-precipitation method. *Phys. Chem. Res.* 3: 191–196.
24. Diaz C., Barrientos L., Carrillo D., Valdebenito J., Valenzuela M. L., Allende P., Geaney H., O'Dwyer C., (2016), Solvent-less method for efficient photocatalytic α-Fe_2O_3 nanoparticles using macromolecular polymeric precursors. *New J. Chem.* 40: 6768–6776.
25. Dos Santos Monteiro D., Da Guarda Souza M. O., (2016), Thermal decomposition of precursors and iron oxide properties: Influence of promoters (Mn and Cu) and preparation method. *J. Therm. Anal. Calorim.* 123: 955–963.
26. De Berti I. O. P., Cagnoli M. V., Pecchi G., Alessandrini J. L., Stewart S. J., Bengoa J. F., Marchetti S. G., (2013),

Alternative low-cost approach to the synthesis of magnetic iron oxide nanoparticles by thermal decomposition of organic precursors. *Nanotechnol*. 24: 175601-175607.
27. Amara D., Grinblat J., Margel S., (2012), Solventless thermal decomposition of ferrocene as a new approach for one-step synthesis of magnetite nanocubes and nanospheres. *J. Mater. Chem.* 22: 2188–2195.
28. Hermankova P., Hermanek M., Zboril R., (2010), Thermal decomposition of ferric oxalate tetrahydrate in oxidative and inert atmospheres: The role of ferrous oxalate as an intermediate. *Eur. J. Inorg. Chem.* 7: 1110–1118.
29. Dey A., Zubko M., Kusz J., Reddy V. R., Banerjee A., Bhattacharjee A., (2019), Solventless synthesis and characterization of α-Fe, γ-Fe, magnetite and hematite using iron(III)citrate. *Solid State Sci.* 95: 105932-105938.
30. Herman D. A. J., Cheong-Tilley S., McGrath A. J., McVey B. F. P., Lein M., Tilley R. D., (2015), How to choose a precursor for decomposition solution-phase synthesis: The case of iron nanoparticles. *Nanoscale*. 7: 5951–5954.
31. Barreiro A., Hampel S., Rümmeli M. H., Kramberger C., Grüneis A., Biedermann K., Leonhardt A., Gemming T., Büchner B., Bachtold A., (2006), Thermal decomposition of ferrocene as a method for production of single-walled carbon nanotubes without additional carbon sources. *J. Phys. Chem. B*. 110: 20973–20977.
32. Sajitha E. P., Prasad V., Subramanyam S. V., Kumar Mishra A., Sarkar S., Bansal C., (2007), Structural, magnetic and Mössbauer studies of iron inclusions in a carbon matrix. *J. Magn. Magn. Mater.* 313: 329–336.
33. Elihn K., Landström L., Alm O., Boman M., Heszler P., (2007), Size and structure of nanoparticles formed via ultraviolet photolysis of ferrocene. *J. Appl. Phys.* 101: 34311-34317.
34. De Souza A. C., Pires A. T. N., Soldi V., (2002), Thermal stability of ferrocene derivatives and ferrocene-containing polyamides. *J. Therm. Anal. Calorim.* 70: 405-409.
35. Shah R., Zhang X. F., An X., Kar S., Talapatra S., (2010), Ferrocene derived carbon nanotubes and their application as electrochemical double layer capacitor electrodes. *J. Nanosci. Nanotechnol.* 10: 4043–4048.
36. Saremi-Yarahmadi S., Tahir A. A., Vaidhyanathan B., Wijayantha K. G. U., (2009), Fabrication of nanostructured α-Fe_2O_3 electrodes using ferrocene for solar hydrogen generation. *Mater. Lett.* 63: 523–526.
37. Kim K.-E., Kim K.-J., Jung W. S., Bae S. Y., Park J., Choi J., Choo J., (2005), Investigation on the temperature-dependent growth rate of carbon nanotubes using chemical vapor deposition of ferrocene and acetylene. *Chem. Phys. Lett.* 401: 459–464.
38. Elihn K,, Larsson K., (2004), A theoretical study of the thermal fragmentation of ferrocene. *Thin Solid Films*. 458: 325–329.
39. Koprinarov N., Konstantinova M., Marinov M., (2010), Ferromagnetic nanomaterials obtained by thermal decomposition of ferrocene. *Solid State Phenom.* 159: 105–108.
40. Nasibulin A. G., Shandakov S. D., Anisimov A. S., Gonzalez D., Jiang H., Pudas M., Queipo P., Kauppinen E. I., (2008), Charging of aerosol products during ferrocene vapor decomposition in N_2 and CO atmospheres. *J. Phys. Chem. C*. 112: 5762–5769.
41. Leonhardt A., Hampel S., Mueller C., Moench I., Koseva R., Ritschel M., Elefant D., Biedermann K., Buechner B., (2006), Synthesis, properties, and applications of ferromagnetic filled carbon nanotubes. *Chem. Vap. Depos.* 12: 380–387.
42. Prakash R., Mishra A. K., Roth A., Kübel C., Scherer T., Ghafari M., Hahn H., Fichtner M., (2010), A ferrocene-based carbon–iron lithium fluoride nanocomposite as a stable electrode material in lithium batteries. *J. Mater. Chem.* 20: 1871–1876.
43. Das B., Kusz J., Reddy V. R., Zubko M., Bhattacharjee A., (2017), Solventless synthesis, morphology, structure and magnetic properties of iron oxide nanoparticles. *Solid State Sci.* 74: 62–69.
44. Das B., Bhattacharjee A., (2018), Kinetic analysis of nonisothermal decomposition of acetyl ferrocene. *Int. J. Chem. Kinet.* 50: 52-61.
45. Cullity B. D., Elements of X-Ray Diffraction, (Addison Wesley, Reading, MA, 1978), p. 102.
46. Snovski R., Grinblat J., Sougrati M. T., Jumas J. C., Margel S., (2014), Synthesis and characterization of iron, iron oxide and iron carbide nanostructures. *J. Magn. Magn. Mater.* 349: 35–44.
47. Chandra Kishore S., Pandurangan A., (2013), Synthesis and characterization of Y-shaped carbon nanotubes using Fe/$AlPO_4$ catalyst by CVD. *Chem. Eng. J.* 222: 472–477.
48. De Boer C. B., Mullender T. A. T., Dekkers M. J., (2001), Low temperature behaviour of haematite: Susceptibility and magnetization increase on cycling through the Morin transition. *Geophys. J. Int.* 146: 201–216.
49. Bhattacharjee A., Roy D., Roy M., Chakraborty S., De A., Kusz J., Hofmeister W., (2010), Rod-like ferrites obtained through thermal degradation of a molecular ferrimagnet. *J. Alloys Compd.* 503: 449-453.
50. Eaton J. A., Morrish A. H., (1969), Magnetic domains in hematite at and above the Morin transition. *J. Appl. Phys.* 40: 3180–3185.
51. Zhang Y. C., Tang J. Y., Hu X. Y., (2008), Controllable synthesis and magnetic properties of pure hematite and maghemite nanocrystals from a molecular precursor. *J. Alloys Compd.* 462: 24–28.
52. Sarangi P. P., Vadera S. R., Patra M. K., Prakash C., Ghosh N. N., (2009), DC electrical resistivity and magnetic property of single phase α-Fe_2O_3 nanopowder synthesized by a simple chemical method. *J. Am. Ceram. Soc.* 92: 2425–2428.
53. Bhattacharjee A., Reiman S., Ksenofontov V., Gütlich P., (2003), Mössbauer spectroscopy under a magnetic field to explore the low-temperature spin structure of the layered ferrimagnetic material—$\{N(n\text{-}C_4H_9)_4[Fe^{II}Fe^{III}(C_2O_4)_3]\}_\infty$. *J. Phys. Condens. Matter*. 15: 5103-5108.
54. Lyubutin I. S., Lin C. R., Korzhetskiy Y. V., Dmitrieva T. V., Chiang R. K., (2009), Mössbauer spectroscopy and magnetic properties of hematite/magnetite nanocomposites. *J. Appl. Phys.* 106: 2–7.
55. Angermann A., Töpfer J., (2008), Synthesis of magnetite nanoparticles by thermal decomposition of ferrous oxalate dihydrate. *J. Mater. Sci.* 43: 5123–5130.
56. Qian W., Chen Q., Cao F., Chen C., (2008), Synthesis and characterization of polyhedral graphite particles. *Open Mater. Sci. J.* 2: 19–22.